Electronic structure of tin dioxide surfaces

S. Munnix and M. Schmeits
Institut de Physique, Université de Liège, Sart Tilman, B-4000 Liège 1, Belgium
(Received 28 October 1982)

We present the results of a theoretical study of the surface electronic structure of the ideal (110), (001), and (100) faces of tin dioxide, a semiconductor crystallizing with the bulk rutile structure. The surface electronic structure is determined using a scattering-theoretic method in which the bulk electronic structure is described by a tight-binding Hamiltonian including first- and second-nearest-neighbor interactions. The results are obtained in terms of surface bound states, surface resonances, and surface densities of states, which are wave-vector, layer, atom, and orbital resolved. All this information allows a detailed discussion of the origin, the nature, and the localization of the obtained surface features. Common trends are found for the three faces. The optical band gap is found to be nearly free of surface states. The dominant features are backbond states in the lower valence-band region and Sn *s*-derived states in the lower conduction-band region. We find one of each for the (001) and (100) faces and two of each for the (110) face which contains two tin atoms per surface unit cell. The upper valence-band region leads only to weak, O *p*-derived resonances. All these features are governed by the relatively strong ionicity of SnO_2. The differences in the results obtained for the three faces are interpreted in terms of the coordination of the surface cations.

I. INTRODUCTION

The electronic structure of semiconductor surfaces and interfaces has been a subject of intense activity during the last ten years. Experimental as well as theoretical studies have shown that the creation of a surface or an interface leads to new characteristic electronic and structural properties, different from those of the constituent bulk phases, thus justifying the fundamental importance of these investigations. Up to now, the main effort was concentrated on semiconductors with diamond, zinc-blende, or wurtzite crystal structure, such as Si, Ge, GaAs, or ZnO for example.

Tin dioxide (SnO_2) is a semiconductor crystallizing in the rutile structure with space group D_{4h}^{14} ($P4_2/mnm$). Its unit cell contains two tin and four oxygen atoms (see Fig. 1). Thus it has a more complex crystalline structure than the compounds mentioned above.

SnO_2 is a material used in numerous technological applications, such as transparent electrodes,[1] gas detectors,[2] far-infrared detectors,[3] and high-efficiency solar cells.[4] As surfaces and interfaces are involved in the mechanisms underlying these devices, a deeper knowledge of their properties would help to improve the understanding of these devices and stimulate the development of new applications.

In the past, bulk properties of SnO_2 have been studied extensively. For a description of general physical properties (preparation, defect structure, electrical and optical properties) we refer to a review article by Jarzebski and Marton.[5] The bulk electronic structure of SnO_2 has been determined by Arlinghaus[6] and by Jacquemin and Bordure.[7] More recently, Robertson[8] has established a tight-binding scheme for the determination of the bulk band structure of semiconducting dioxides, including SnO_2. Surface properties of SnO_2, however, have received only little attention. Experimentally, they were studied by de Frésart *et al.*,[9] who performed

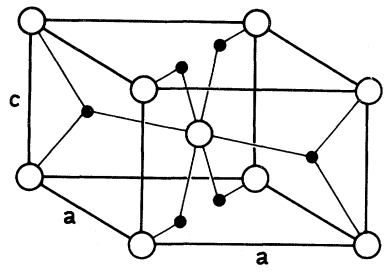

FIG. 1. Bulk unit cell of SnO_2. Open circles represent Sn atoms; dark circles, O atoms.

low-energy electron diffraction (LEED) analysis, Auger-electron emission, and surface conductivity measurements on different natural faces. To our knowledge, no theoretical results have been reported up to now on the SnO_2 surface electronic structure. This may be due to the complexity of the rutile crystal structure, which makes the application of standard theoretical methods unpractical.

The present paper is devoted to the theoretical determination of tin dioxide surface electronic structures. We present the results of a systematic study of a series of low-index faces of SnO_2: The (110), (001), and (100) faces are investigated. For each face, we consider one atomic configuration, and assume that the atoms are held at their bulk ideal positions.

Of course, for a given face different surface compositions are possible as the crystallographic structure of SnO_2 allows us to terminate the semi-infinite crystal by different atomic planes. Depending on how the crystal is "cut," the surface-layer composition may differ from one case to another. The surface-layer models we have chosen have a composition which is favored by the Auger analysis done by de Frésart *et al.*[9]

Furthermore, the surface may relax or reconstruct, leading to new atomic positions different from those in the perfect bulk crystal. At present, however, no detailed experimental results are available from which the exact atomic configuration could be unambiguously deduced. LEED measurements show for each face several reconstruction phases depending on the treatment of the surface.[9] But the observation of (1×1) LEED patterns for each of the faces considered here shows the unreconstructed surface to be a stable phase.

Of course, even in this case the occurrence of relaxation is probable, but this will not strongly modify the surface electronic features, as it results from previous studies on surface relaxation effects for materials of comparable ionicity.[10] We are thus able to determine the characteristic features of each face and analyze the behavior of each surface electronic state. As will be shown, this behavior is governed by the ionicity of the material and by the atomic coordination of the surface cations.

Our calculations are carried out by making use of the scattering-theoretical method[11] which will be referred to in the following as STM. This method has already been applied successfully to ideal, relaxed, and reconstructed surfaces of Si, Ge, GaAs, InSb, or ZnO.[10–12]

One major advantage of the STM is to yield directly the electronic structure of the semi-infinite crystal. Moreover, in alternative calculations, using slab or cluster methods, large-sized slabs or clusters have to be utilized in order to yield reliable results. This requires heavy numerical calculations involving large matrices. In the STM the dimensions of the matrices to be handled depend essentially on the perturbation introduced to "create" the surface. With the use of a Hamiltonian with interactions up to second-nearest neighbors, only a few layers have to be removed in order to produce a complete decoupling of the resulting two surfaces. Thus the problem remains numerically tractable, even for crystals such as SnO_2, with six atoms per bulk unit cell.

We obtain our results in terms of bound surface states, surface resonances, and surface densities of states. The local densities of states obtained by the STM are resolved with respect to surface wave vector, layer, atomic position, and orbital composition. These results allow a detailed analysis of the various features, revealing their localization, their origin, and their atomic and orbital character.

The outline of the paper is as follows: In Sec. II, we review the bulk electronic properties of SnO_2. In Sec. III, the general formalism of the STM is briefly described. In Sec. IV we present the results for the (110), (001), and (100) surfaces. In Sec. V we discuss these results and compare them for the different faces. Section VI concludes this paper.

II. BULK ELECTRONIC STRUCTURE OF SnO_2

In this section we briefly sum up the main characteristics of the bulk band structure of SnO_2, as it constitutes a necessary background to interpret the surface electronic states. The bulk unit cell of SnO_2 is shown in Fig. 1. It is of tetragonal symmetry, with a quadratic basis of side $a=4.737$ Å and a height of $c=3.186$ Å. It contains two tin and four oxygen atoms. The oxygen atoms are at position $(\pm ua,\pm ua,0)$ respective to the nearest tin atom, with $u=0.307$. Each tin atom is surrounded by a distorted octahedron of six oxygen atoms and each oxygen atom has three tin nearest neighbors at the corners of an almost equilateral triangle.

We describe the bulk band structure by a tight-binding Hamiltonian which defines bulk Bloch functions $\Psi_{n,\vec{k}}(\vec{r})$ as linear combinations of atomic orbitals (LCAO) $\varphi_\alpha(\vec{r})$ according to

$$\Psi_{n,\vec{k}}(\vec{r})=\sum_{\alpha,\nu} C^n_{\alpha\nu}(\vec{k})\chi^{\alpha\nu}_{\vec{k}}(\vec{r}) , \tag{1}$$

with

$$\chi^{\alpha\nu}_{\vec{k}}(\vec{r})=\frac{1}{\sqrt{N_3}}\sum_j \exp[i\vec{k}\cdot(\vec{R}_j-\vec{\tau}_\nu)] \times\varphi_\alpha(\vec{r}-\vec{R}_j-\vec{\tau}_\nu) . \tag{2}$$

In these expressions, $\vec{R}_j$ is a Bravais lattice vector and $\vec{\tau}_\nu$ specifies the positions of the atoms in the unit cell. N_3 is the number of lattice points in the normalization volume of the Bravais lattice.

For SnO_2 we have adopted the tight-binding scheme of Robertson,[8] which has established a parameter set for a series of non-transition-metal compounds with the rutile structure. For SnO_2 the orbital index α runs over the $2s$ and $2p$ orbitals for O and over the $5s$ and $5p$ orbitals for Sn, as the chemical bonding is mainly governed by these orbitals. The parameter set, which has been slightly modified, includes interactions up to second-nearest neighbors. This leads to a 24×24 Hamiltonian matrix, whose diagonalization yields the energy dispersion relations $E_n(\vec{k})$ as well as the wave functions $\Psi_{n,\vec{k}}(\vec{r})$. A schematic view of the resulting bulk band structure is shown in Fig. 2. We display the contributions from the four orbital types included in the tight-binding scheme.

The band located around -17 eV originates essentially from oxygen s states, with a very small fraction of Sn s and Sn p admixture. As it is separated by a 7-eV-wide gap from the upper valence band, these states are only weakly coupled to the higher bands, which are of interest in our study. For this reason, the O s band will not be considered in greater detail in the following discussion.

The main valence band is 9 eV wide, in agreement with UPS measurements by Gobby.[13] It may be divided into three parts of different orbital composition. The region between -9 and -5 eV results from a coupling of Sn s orbitals to O p orbitals. The latter have essentially a "bonding-p" character, i.e., they are directed along the nearest-neighbor Sn-O axis and appreciably contribute to the chemical bonding. This strong s-p interaction produces a high dispersion of these bands. The bands in the region between -5 and -2 eV consist of oxygen bonding-p orbitals mixed with a smaller fraction of Sn p orbitals. The region between -2 eV and the valence-band edge (0 eV) consists mainly of O p "lone-pair" orbitals, which are directed perpendicularly to the Sn-O axis and contribute little to chemical bonding. Owing to their weak interaction with other orbitals, they give rise to quite flat bands yielding a strong peak in the density of states. The top of the valence band is a state of Γ_3^+ symmetry, in agreement with two-photon spectroscopy measurements by Fröhlich *et al.*[14]

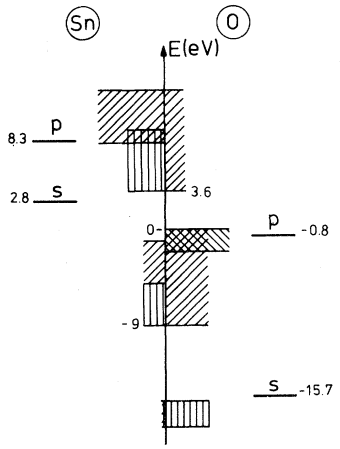

FIG. 2. Schematic draft of valence and conduction bands of SnO_2. The top of the valence band is at 0 eV. The dominant orbital character for the different band groups is indicated as follows: Sn s (| | |), Sn p (///), O s (| | |), O bonding p (///), O lone-pair p (\ \ \).

The band gap has a width of 3.6 eV, according to most measurements made up to date.[15] The bottom of the conduction band, from 3.6 to 8 eV, is made to 90% of Sn s states with a strong dispersion, giving rise only to a low density of states. The top of the conduction band has a dominant Sn p character. It should be mentioned that all states in the conduction band also contain a small admixture of O p bonding orbitals. This bulk electronic structure serves as input for the STM, which we will describe shortly in the next chapter.

III. GENERAL FORMALISM

The detailed formal developments of the STM can be found in Ref. 11. For the sake of completeness, we shall recall the essential steps leading to the final expressions to be used in numerical computations. The STM uses the Green's function G^b associated with the bulk Hamiltonian H^b of the crystal. G^b is defined as

$$G^b(E)=\lim_{\epsilon\to0+}(E+i\epsilon-H)^{-1}=\sum_{n,\vec{k}}\frac{|n,\vec{k}\rangle\langle n,\vec{k}|}{E^+-E_n(\vec{k})}\ , \tag{3}$$

where $|n,\vec{k}\rangle$ and $E_n(\vec{k})$ are, respectively, the eigenvectors and eigenvalues of H^b and where E^+ stands for $E+i\epsilon$, with $\epsilon\to0+$. The matrix elements of G^b are written in a basis which exploits at best the symmetry of the problem. Because of the surface-parallel two-dimensional translational symmetry, the wave functions may be expressed as Bloch sums of layer orbitals and constitute the "layer orbital" basis:

$$\langle\vec{r}\,|\,m,\alpha,\mu;\vec{q}\,\rangle=\frac{1}{\sqrt{N_2}}\sum_j e^{i\vec{q}\cdot(\vec{\rho}_j+\vec{\lambda}_\mu^m)}\varphi_\alpha(\vec{r}-\vec{\rho}_j-\vec{\lambda}_\mu^m)\ . \tag{4}$$

In this expression $\vec{q}$ is a two-dimensional wave vec-

tor, $\vec{\rho}_j$ is a lattice vector of the two-dimensional Bravais lattice, and $\vec{\lambda}_\mu^m$ is the position in the unit cell of the atom μ located in the mth layer. N_2 is the number of lattice points contained in the normalization area. $\varphi_\alpha(\vec{r})$ is an atomic orbital of type α centered on $\vec{r}=0$, as already used in the LCAO development of Eq. (2).

The vector $\vec{\lambda}_\mu^m$ can be decomposed into a surface-parallel component $\vec{\sigma}_\mu^m$ and a surface-perpendicular component $\vec{\kappa}^m$ according to

$$\vec{\lambda}_\mu^m=\vec{\sigma}_\mu^m+\vec{\kappa}_m \ . \tag{5}$$

Introducing the composite index $l=(m,\alpha,\mu)$, the bulk Green's function is given in the layer orbital representation by

$$G_{ll'}^b(\vec{q},E)=\sum_{n,\vec{k}}\frac{\langle l,\vec{q}\mid n,\vec{k}\rangle\langle n,\vec{k}\mid l',\vec{q}\rangle}{E^+-E_n(\vec{k})} \ , \tag{6}$$

which may be transformed into[11-12]

$$G_{ll'}^b(\vec{q},E)=\frac{N_2}{N_3}\sum_{\vec{g}}{}'\sum_{\vec{k}_\perp}{}'\exp[i\vec{k}_\perp\cdot(\vec{\kappa}_m-\vec{\kappa}_{m'})]\exp[i\vec{q}\cdot(\vec{\sigma}_\mu^m-\vec{\sigma}_{\mu'}^{m'})]\sum_n\frac{C_l^n(\vec{q}+\vec{g},\vec{k}_\perp)C_{l'}^{n*}(\vec{q}+\vec{g},\vec{k}_\perp)}{E^+-E_n(\vec{q}+\vec{g},\vec{k}_\perp)} \ . \tag{7}$$

In this equation $\vec{q}$ is in the surface Brillouin zone, $\vec{k}_\perp$ is a wave vector perpendicular to the surface, and $\vec{g}$ is a vector of the two-dimensional reciprocal lattice. For a given $\vec{q}$ the sums over $\vec{g}$ and $\vec{k}_\perp$ run over those values for which $\vec{k}=\vec{q}+\vec{g}+\vec{k}_\perp$ lies inside the first bulk Brillouin zone.

For each of the three faces under study, Eq. (7) can be transformed in order to eliminate the sum over $\vec{g}$ and to reduce the sum over $\vec{k}$ to a single integral, with its integration range independent of $\vec{q}$. This yields (see the Appendix)

$$G_{ll'}^b(\vec{q},E)=\frac{1}{2\beta}\int_{-\beta}^{+\beta}\exp[ik_\perp(d_m-d_{m'})]\times F_{ll'}(k_\perp,\vec{q},E)dk_\perp \ , \tag{8a}$$

where

$$F_{ll'}(k_\perp,\vec{q},E)=\sum_n\frac{C_l^n(\vec{q},k_\perp)C_{l'}^{n*}(\vec{q},k_\perp)}{E^+-E_n(\vec{q},k_\perp)} \tag{8b}$$

and

$$\beta=\begin{cases}\dfrac{\pi}{a} & \text{for the (100) face}\\ \dfrac{\pi\sqrt{2}}{a} & \text{for the (110) face}\\ \dfrac{\pi}{c} & \text{for the (001) face.}\end{cases} \tag{8c}$$

$d_m-d_{m'}$ is the distance separating layers m and m'.

It is worthwhile mentioning that for each of the faces, the area of the corresponding Brillouin zone multiplied by the integration interval length 2β yields the volume of the bulk Brillouin zone, expressing the conservation of the total number of states.

The surface is "created" by removing as many atom layers as are necessary in order to decouple the two remaining semi-infinite solids. This is achieved by adding to the bulk Hamiltonian a short-range perturbation, whose representation in the layer orbital basis is

$$U_{ll'}=\begin{cases}\lim\limits_{u\to\infty}u\delta_{\alpha\alpha'}\delta_{\mu\mu'}\delta_{mm'} & \text{if } m \text{ is the removed layer}\\ 0 & \text{otherwise.}\end{cases} \tag{9}$$

This sets the atomic energy levels on the removed atoms to infinity and thus reduces their interactions with the remaining crystal atoms to zero.

The effective dimensions of the perturbation matrix depend on the number of atoms to be removed. For rutile-type crystals with second-nearest-neighbor interactions included in the tight-binding scheme, U has dimensions of the order of 24×24. The STM also has the advantage of giving the electronic structure of a "true" surface, i.e., the abrupt transition between a half space filled by the crystal and a half space of vacuum. In slab methods, on the contrary, there may be an interference between the states originating from the two limiting surfaces, if these states extend over a distance of the order of the slab thickness. In the case of cluster methods, no surface-parallel periodicity is included, which makes resolution with respect to wave number a difficult task, and redundant surfaces may introduce additional boundary effects.

If one projects the bulk bands onto the surface Brillouin zone, one obtains, for each $\vec{q}$, energy regions filled with bulk states, alternating with empty gaps or pockets. Two types of surface features may occur: true surface states, which are localized in the gaps or pockets, and resonances, which are peaks in the change of density of states, localized inside the bulk bands.

The surface states are obtained as solutions of the equation[11]

$$D(\vec{q},E)\equiv\det|-G^b_{ij}(\vec{q},E)|=0\,, \tag{10}$$

where the indices i and j are restricted to the subspace of removed atoms.

Local surface densities of states can be obtained as partial traces of the surface Green's function G^s according to

$$\mathcal{N}_l(\vec{q},E)=-\frac{1}{\pi}\mathrm{Im}G^s_{ll}(\vec{q},E)\,. \tag{11}$$

This surface Green's function is obtained by solving Dyson's equation

$$G^s(\vec{q},E)=G^b(\vec{q},E)+G^b(\vec{q},E)UG^s(\vec{q},E)\,, \tag{12}$$

with U given by Eq. (9) for the ideal surface. The solution is expressed as

$$\mathcal{N}_l(\vec{q},E)=-\frac{1}{\pi}\mathrm{Im}\left[G^b_{ll}(\vec{q},E)-\sum_{i,j}G^b_{li}(G^b_{ij})^{-1}G^b_{jl}\right], \tag{13}$$

where the indices i and j range over the subspace of the perturbation U. By taking the sum over a more or less restricted set of values, one obtains layer, atom, or orbital resolved densities of states, which allow a detailed analysis of the nature and the localization of each surface-induced feature.

Equation (13) contains two terms, the first being the bulk density of states and the second being the surface-induced change in the bulk density of states. We shall now apply the STM to obtain the results outlined above in the case of the (110), (001), and (100) ideal faces of SnO_2.

IV. RESULTS OF SnO_2 SURFACE ELECTRONIC STRUCTURES

A. The SnO_2 (110) surface

We have shown the surface unit cell of the (110) surface in Fig. 3. As the outer plane, we have chosen the one containing two tin and two oxygen atoms, i.e., the plane of highest atomic density. This is also strongly supported by Auger measurements performed by de Frésart *et al.*[9] On the first layer ($m=1$), the central atom Sn_1 is of coordination 4, i.e., it has lost two of its nearest-neighbor oxygen atoms, whereas Sn_2, having lost only one, is of coordination 5. The surface oxygen atoms O_1 and O_2 retain all their bulk nearest neighbors (coordination 3). In the subsurface layer ($m=2$), there is only one oxygen atom O_3 per unit cell, which is bound to two Sn_1 atoms in layer $m=1$ and to one Sn_2 atom in layer $m=4$. The atom O_4 in the third layer has the symmetric environment of atom O_3, i.e., the plane $m=4$ plays the same role for atom O_4 as the plane $m=1$ plays for atom O_3. The fourth layer is identical to the first one, up to a surface-parallel translation by $(a/\sqrt{2},0)$.

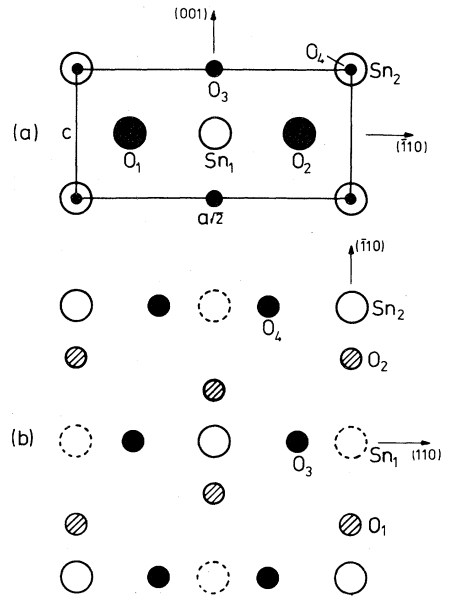

FIG. 3. Surface unit cell of SnO_2(110). (a) top view, (b) side view. The atoms Sn_1, Sn_2, O_1, and O_2 are in the surface layer; O_3 and O_4 are, respectively, in the second and third layer.

In Fig. 4 we display the projected bulk electronic structure and the surface bands for the (110) face.

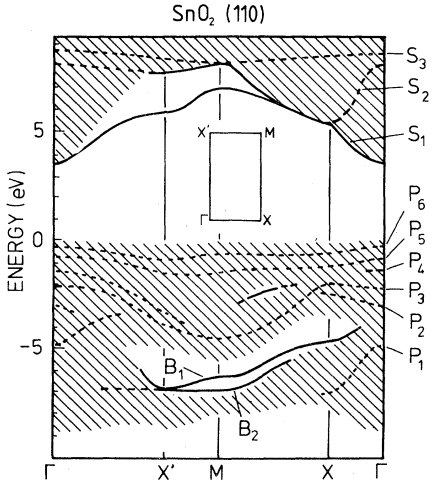

FIG. 4. Projected bulk band structure and surface band structure of the ideal SnO_2(110) surface. Inset: irreducible part of the (110) surface Brillouin zone.

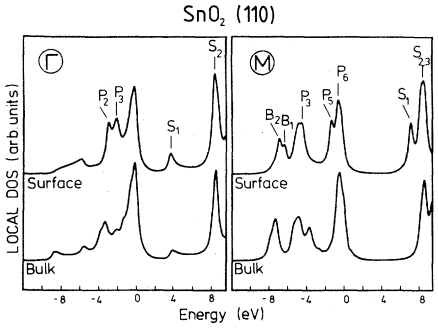

FIG. 5. Wave-vector-resolved densities of states for the surface layer of ideal $SnO_2(110)$ in comparison with the DOS of the corresponding bulk layer for the high-symmetry points Γ and M. Features localized on subsurface layers do not appear on this figure. All DOS's have been calculated with a 0.3-eV Lorentzian broadening.

The most pronounced resonances are also shown, as dashed lines. Figure 5 shows the wave-vector-resolved density of states (DOS) at the high-symmetry points Γ and M, summed up over the four atoms on the surface layer. In the same figure, we show the bulk DOS corresponding to that layer. These layer densities of states not only reveal the energetic positions of the surface states and resonances, as they appear as peaks or shoulders in the DOS spectrum, but also allow one to evaluate the strength of a projected bulk band region, as well as of a surface-induced feature.

Let us now discuss in some detail the different states observed. The O s band has not been included as it is only weakly coupled to the upper valence bands and is outside the energy range accessible to most of surface sensitive experiments presently available. The states B_1 and B_2 are located in the pocket between -7.5 and -5 eV. They have an important Sn s contribution from atoms Sn_1 and Sn_2, respectively, and a strong p contribution from the two subsurface oxygen atoms. This identifies them clearly as backbond states, which are localized in the region of the two first layers. At X', the states B_1 and B_2 are degenerate, and for other q values, B_1 lies at higher energies than B_2, a fact we will explain later on.

In the upper valence-band region, we have outlined six resonances, whose strengths are, however, quite variable through the Brillouin zone and relatively weak as compared to resonances arising at surfaces of more covalent materials. The nature of these states is mainly of O p character, but their localization changes throughout the Brillouin zone. For instance, at M, P_5 is mainly due to oxygen states on the surface atoms O_1 and O_2, whereas at X, it originates from the subsurface atom O_3.

The optical band gap is nearly free of surface states. In the conduction-band region, we have denoted three states S_1, S_2, and S_3. S_1 has a dominant contribution from Sn_1 s orbitals, whereas S_2 has mainly Sn_2 s character. S_3 is degenerate with S_2 at M and has a dominant Sn p composition. It already originates from the higher conduction bands.

The fact that S_1 is separated more strongly from the conduction band than S_2 is related to the same argument which explains the larger energy shift of B_1 relative to B_2; S_1 and B_1 are both located on Sn_1, whose coordination is 4. S_2 and B_2 are located on Sn_2 which is of coordination 5. Thus, Sn_2 having a more "bulklike" environment than Sn_1, the states S_1 and B_1 tend to shift more strongly outward from the bulk energy region from which they are issued.

B. The SnO_2 (001) surface

The geometry of the surface unit cell is shown in Fig. 6. Each layer contains one tin and two oxygen atoms, which are aligned along one of the diagonals of the surface unit cell. The layers are separated from one another by $c/2$. Two successive layers are identical, but rotated by 90° with respect to one another. The atoms of the surface layer ($m=1$) are labeled Sn_1, O_1, and O_2, those of the second layer ($m=2$) are labeled Sn_2, O_3, and O_4.

In Fig. 7 we show the surface band structure of the (001) face along the symmetry lines of its Brillouin zone. It should be noted that, due to the bulk symmetry, the projected bulk bands are symmetric

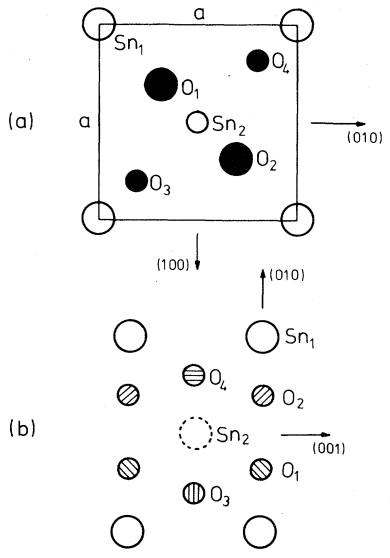

FIG. 6. Top view (a) and side view (b) of the $SnO_2(001)$ surface. The atoms Sn_1, O_1, and O_2 are in the surface layer; Sn_2, O_3, and O_4 are in the subsurface layer.

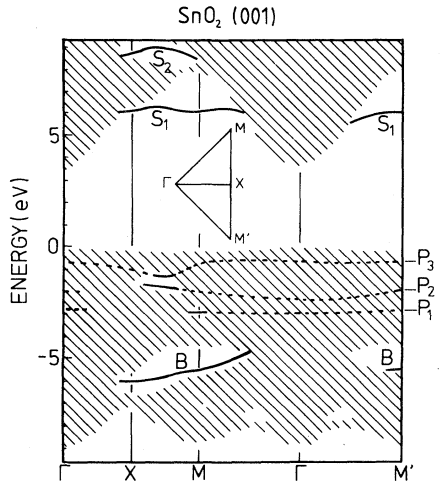

FIG. 7. Projected bulk band structure and surface band structure of $SnO_2(001)$. Inset: irreducible part of the (001) surface Brillouin zone (SBZ).

with respect to the ΓX axis. But no longer are the surface bands, due to the loss of translational symmetry along c. These facts are reflected in Fig. 7. However, the band structures at M and M' are identical by two-dimensional translational symmetry.

Figure 8 displays, for the three high-symmetry points Γ, X, and M, the layer density of states on the three outermost layers in comparison with the bulk density of states. In general, for an arbitrary $\vec{q}$ value, the projected bulk DOS on the odd layers differs from that on the even ones, due to the different orientation of the atomic arrangement. At the high-symmetry points considered, however, it can be easily seen that through point and translational symmetry, all layers are equivalent from the bulk point of view. Figure 8 allows one to follow the evolution of the layer DOS from the surface

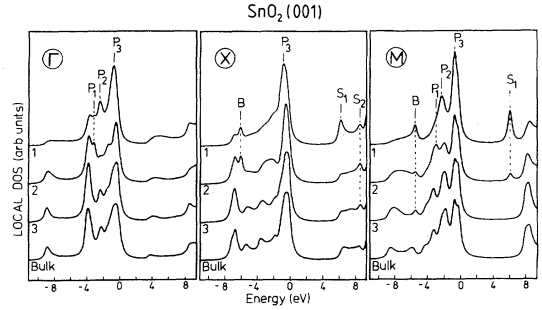

FIG. 8. Wave-vector-resolved DOS for the three outer layers of $SnO_2(001)$ in comparison with the DOS of the corresponding bulk layer for the three high-symmetry points Γ, X, and M.

layer toward a bulk layer. On layer three, it already approaches the bulk DOS.

At Γ, no surface state emerges from the projected bulk DOS, the peak structure being nearly the same for surface and bulk. In the small pocket gap which appears between -7 and -5 eV, there is one state we have labeled B. It is localized on the outermost layer, where it is made at 60% of Sn s orbitals, and on the second layer, where it consists of 75% O p orbitals. Thus we have again a backbond state, which is due to the cut of s-p interactions between the surface Sn and its O first-nearest neighbors on the removed layers, leaving an Sn atom of coordination 4. The backbond band follows closely the lower border of the pocket, with a maximum separation of 0.7 eV at X. Contrary to the (110) face, we have only one B state, as now all Sn atoms at the surface are equivalent.

The resonances labeled P, in the upper part of the valence band, are of O p character and are localized on the two outer layers. As for the (110) face, they are relatively weak, despite the fact that each surface oxygen has now lost one tin nearest neighbor. This is related to the relatively strong ionicity of the material, which makes the surface creation produce only moderate charge rearrangements.

The gap is again completely free of surface states, surface features occurring only above approximately 6 eV. The first of these, S_1, lies outside the projected conduction band and disappears near the center of the Brillouin zone, around Γ. It has a dominant

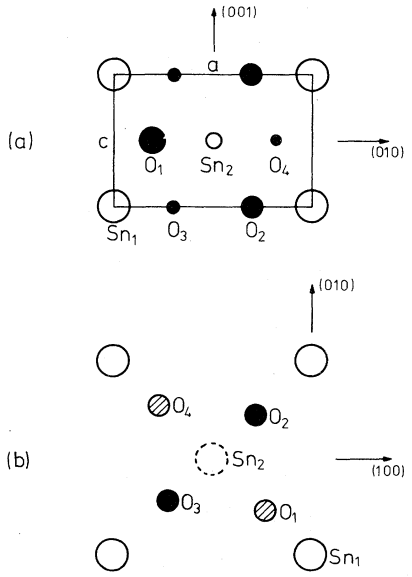

FIG. 9. Top view (a) and side view (b) of the $SnO_2(100)$ surface. The atoms Sn_1, O_1, O_2, Sn_2, O_3, and O_4 are, respectively, in the layers 1 to 6.

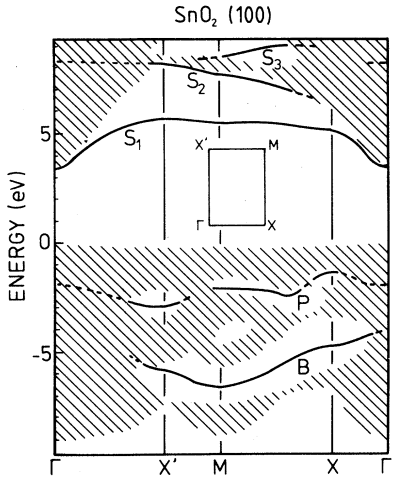

FIG. 10. Projected bulk band structure and surface band structure of $SnO_2(100)$. Inset: irreducible part of the (100) SBZ.

Sn s character and is localized predominantly on the outer layer. S_2 is a state in the small pocket above 8 eV already having an important Sn p contribution. Its amplitude is, however, far smaller than that of S_1.

C. The $SnO_2(100)$ surface

The unit cell of the (100) face is displayed in Fig. 9. Each atomic plane contains one atom per surface unit cell. We have terminated the surface by the Sn plane. The surface tin atom is of coordination 3. The following two layers contain one oxygen atom each, and the three next layers are equivalent to the three first ones, up to a translation by $(a/2,c/2)$.

The surface band structure we have computed is displayed in Fig. 10. Figure 11 shows, for point X of the surface Brillouin zone (SBZ), the atomically resolved surface density of states on the first six layers, as well as the corresponding changes in the bulk DOS induced by the surface. The valence band presents a wide pocket which contains a state labeled B. Just as for the other faces, this state is again a backbond state, extending over the surface tin and the subsurface oxygen atoms. It disperses nearly parallel to the lower border of the pocket and reaches a separation of 1.4 eV at X' and 1 eV at X, which is quite stronger than for the (110) and (001) faces. This is clearly related to the low coordination of the surface Sn which has lost 50% of its nearest-neighbor oxygen atoms.

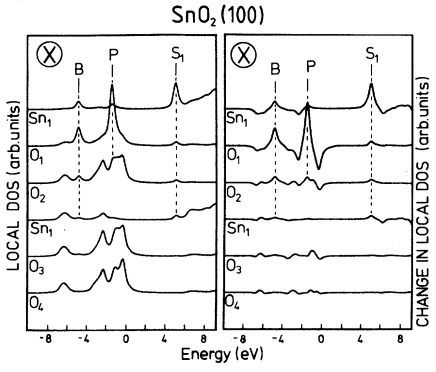

FIG. 11. Atomically resolved DOS (left) and change in DOS with respect to the bulk (right) at X for the six atoms in the six outer layers of the (100) surface.

The small gaps in the top region of the valence band, around -2 eV, contain a state labeled P, which persists inside part of the bulk bands as a resonance. This state again has p character and is localized on the subsurface oxygen atom O_1. The p-orbital character changes with q, but the dominant contribution is p_z, i.e., directed perpendicularly to the surface. Since the environment of O_1 is relatively open toward the surface, this state has some dangling bond character and is mainly due to the suppression of $V_{pp\sigma}$ interactions between Sn p and O p orbitals. On this surface fewer P resonances are present, as no oxygen atoms are contained in the outer layer. In the lower conduction-band region, we have found three features labeled S_1, S_2, and S_3. S_1, the lowest of these, has again a dominant Sn s orbital character and is localized mainly on the outer Sn atom. As compared to the corresponding S states in the two other faces, it has less dispersion and separates far more from the conduction-band edge, reaching up to 2.7 eV at X'. This behavior is due to the lower coordination of the surface Sn atom on this face. The states S_2 and S_3 are of less pronounced amplitude. S_2, being mainly composed of Sn_2 s states and Sn_1 p_y states, is a faint analog of the S_2 state on the (110) face. S_3 has dominant Sn p character and, though being a true surface state in the conduction-band pocket, is only of very weak DOS amplitude.

V. COMPARISON OF THE THREE SURFACE ELECTRONIC STRUCTURES

The results we have obtained for the three model surfaces can be summarized as follows:

(1) For the three faces, the gap is nearly free of surface states.

(2) In the lower valence-band region, a pocket opens in the projected bulk band, in which we have found one backbond state B for the (001) and the (100) face and two backbond states B_1 and B_2 for the (110) face, as this latter face contains two tin atoms per surface unit cell.

(3) In the upper valence-band region, i.e., between -4 and 0 eV, we have found for each face several O p resonances of relatively weak intensity.

(4) In the lower conduction-band region, we observe one S state for the (001) and (100) faces and two S states for the (110) face. These states have a dominant Sn s character on the surface Sn atoms.

These surface electronic features can be understood with the help of the bulk electronic structure we have recalled in Sec. II.

The ionicity of the material is implicitly correlated with the diagonal matrix elements of the constituting atoms. For homopolar or weakly polar tetrahedrally bonded semiconductors, the atomic s and p states hybridize into sp^3 orbitals whose energy levels are inside the gap of the resulting crystal.[16] The creation of a surface is realized through suppression of first- and second-nearest-neighbor interactions. As a consequence, bulk valence or conduction states are modified, shifting toward the isolated atom energy levels. This leads for ideal surfaces to the well-known dangling bond states inside the gap.

Tin dioxide is a semiconductor of relatively strong ionicity. On the Phillips ionicity scale, the ionicity has been estimated to $f_i=0.78$, as compared to 0.32 for GaAs or 0.65 for ZnO.[17] The ionic character is even reinforced by the crystallographic structure of SnO_2, where not all the valence oxygen p electrons contribute to the crystal binding. The lone-pair p orbitals, oriented perpendicular to the Sn-O-Sn planes, couple only weakly through $V_{pp\pi}$ interactions with the neighboring Sn atoms and through second-nearest-neighbor interactions with other oxygen atoms.[8] Henceforth, the lone-pair electrons build an ionic charge closely localized to the oxygen nuclei. These lone-pair states lead to weakly dispersing bands whose energy is close to the atomic oxygen p level and which constitute the major contribution to the upper valence band density of states.

As one can see from Fig. 2, where we have shown the schematic bulk density of states, the resulting bulk band structure is such that in our parametrization scheme, the diagonal O s and O p levels are below the top of the valence band, E^s_{Sn} is 0.8 eV below the conduction-band edge E_c, and E^p_{Sn} is well above E_c. If a surface is created, the shift of bulk states through new combinations of atomic states cannot lead to dangling bond states inside the gap. As we effectively have found, only the S_1 states on the (110) and (100) surfaces are 0.1 eV below the conduction-band minimum for q values close to Γ. In addition, these S_1 states are of dominant Sn s orbital composition, not having the characteristic dangling bond character. Furthermore, oxygen-derived dangling bond states will not occur as the lone-pair states dominating the upper valence-band region are nearly unaffected by a modified environment and bonding O p orbitals yield bulk states which are mostly situated more than 2 eV below the top of the valence band.

We turn now to the discussion of the surface states effectively present. As illustrated in Fig. 2, the lower part of the valence band (-9 to -5 eV), as well as the lower part of the conduction band (3.6 to 9 eV), result, respectively, from bonding and antibonding combinations of Sn s and O p orbitals, modulated by a strong V_{sp} interaction.[8] The creation of a surface leads to the new states B and S_1 on the surfaces having one Sn atom per surface unit cell and to the states B_1, B_2, S_1, and S_2 for the (110) surface, which has two nonequivalent Sn atoms per surface unit cell. As the B states are composed mainly of Sn s states on the surface layer and O p states on the subsurface layer, they have been called backbond states. Calling their counterparts $S_{1,2}$, originating from the antibonding bulk-state region, antibackbond states is an open question, as their contribution from the subsurface layer is rather weak.

The shift of these states, respective to the bulk states from which they are derived, depends on the coordination of the surface atoms. This is illustrated in Table I, where we have shown for the three surfaces under study, the coordination of each surface Sn atom together with the maximum shift of each of the states B and S respective to the bulk band regions from which they originate. This maximum shift is, as Figs. 4, 7, and 10 show, an indica-

TABLE I. Maximum separation with respect to the projected bulk band edges for the different backbond B states and Sn s-derived S states.

Face	Atom	Coordination	B states	S states
(110)	Sn_2	5	B_2 : 0.25 eV (M)	S_2 : 0.05 eV (X')
	Sn_1	4	B_1 : 0.8 eV (M)	S_1 : 2 eV (X')
(001)	Sn_1	4	B : 0.7 eV (X)	S_1 : 1.75 eV (M)
(100)	Sn_1	3	B : 1.40 eV (X')	S_1 : 2.7 eV (X')

tion of the separation of each surface state respective to the projected bulk band edge. The shifts increase with decreasing coordination, i.e., with the number of suppressed V_{sp} interactions.

The Sn_1 atoms on the faces (110) and (001) have the same coordination 4, but the shifts of the states B and S_1 are different by about 0.2 eV. This difference might result, in addition to geometrical reasons, from the fact that on the (110) surface, the two Sn atoms interact, which leads to a repulsion of the states B_1 and B_2, and S_1 and S_2, respectively. From the DOS of the (110) surface (see Fig. 5), one can effectively see that the states B_1 and B_2 (S_1 and S_2) have nonzero amplitudes on both of the surface cations. Another consequence of this Sn-Sn interaction is that the states B_2 and S_2 are relatively close to the edge of the projected bulk band states.

The shift of the S states is stronger than that of the B states, as the S states move from the lower conduction-band edge toward a large empty gap. The B states, on the contrary, feel the influence of the states in the region above the pocket which exists around -5 eV. The different oxygen p resonances are only weak in intensity and their localization and orbital character varies with surface wave vector $\vec{q}$. When located below -1.5 eV, they are due to the suppression of $V_{pp\sigma}$ interactions between nearest-neighbor O and Sn p orbitals. Those located above -1.5 eV are due to the suppression of second-nearest-neighbor O-O interactions and first-nearest-neighbor $V_{pp\pi}$ interactions.

This closes the discussion of the behavior of the different surface electronic features we have observed. The electronic structure of SnO_2 surfaces shows close analogy with the electronic structure of ZnO surfaces.[10,18] Indeed, for ZnO surfaces no gap states were found and the dominant features are backbond and antibackbond states. Apart from differences resulting from the inclusion of Zn d orbitals in Ref. 18, the conclusions are similar, as the ionicity of both materials is of the same order of magnitude. The valence and conduction bands of SnO_2 and ZnO originate from the same atomic orbital states; the differences in the bulk and surface electronic structures result from the underlying crystallographic structure and the chemical nature of the cations.

VI. CONCLUSION

We have studied the surface electronic structure of the ideal SnO_2 (110), (001), and (100) surfaces. We have used the scattering-theoretic method which has proved its efficiency also when applied to semiconductors of relatively complicated crystallographic structure, like the rutile structure in our case. As results, we obtain the bound surface states, surface resonances, and local densities of states. The characteristic surface features are governed by the ionicity of the material and the coordination of the surface atoms.

For each face, we have determined the surface electronic structure for one given atomic composition of the surface. Results for different atomic compositions can be obtained easily within the used STM, as the computation of the bulk Green's function has to be performed only once, the perturbation U only has to be modified for each surface model. A systematic analysis of the variation of the electronic structure with surface composition is presently under study.

We have also restricted ourselves to the ideal surface case. Extension of our results to relaxed and reconstructed surfaces is possible within the framework of the STM,[12] provided the surface atomic positions are known, which is not the case for SnO_2 presently. But, as already mentioned in the Introduction, no drastic changes in the surface densities of states are to be expected. The strongly ionic character of SnO_2 leads already to surface electronic charge distributions which are relatively stable, as no dangling bonds call for a strong rearrangement of surface atomic and electronic structure. These conclusions were also drawn by Ivanov and Pollmann,[10] who showed that for ZnO the ideal surface densities of states were already in very good agreement with experiment.

For SnO_2, no comparison with experiment is possible at the present time since, to our knowledge, no photoemission or electron energy-loss experiments were reported in the literature. In particular, angle-resolved or angle-integrated UPS measurements would help to contribute to the understanding of the detailed bulk and surface electronic structure of tin dioxide.

ACKNOWLEDGMENTS

We are grateful to Dr. J. Robertson for helpful correspondence as well as to Professor J. M. Gilles and Dr. E. de Frésart for useful discussions. One of us (S.M.) would like to thank the Belgian Fonds National de la Recherche Scientifique (FNRS) for financial support.

APPENDIX: EVALUATION OF THE GREEN'S-FUNCTION MATRIX ELEMENTS

In this appendix we derive the expression of the Green's-function matrix elements listed in Eqs. (7)

and (8). Detailed calculations are made for the (110) face only, which is the least trivial case. The corresponding results for the other faces are straightforward.

The general expression of the Green's-function matrix element is given by Eq. (7):

$$G^b_{ll'}(\vec{q},E)=\frac{N_2}{N_3}\sum_{\vec{g}}{}'\sum_{\vec{k}_\perp}{}'\exp[i\vec{k}_\perp\cdot(\vec{\kappa}_m-\vec{\kappa}_{m'})]\exp[i\vec{q}\cdot(\vec{\sigma}^m_\mu-\vec{\sigma}^{m'}_{\mu'})]\sum_n\frac{C^n_l(\vec{q}+\vec{g},\vec{k}_\perp)C^{n*}_{l'}(\vec{q}+\vec{g},\vec{k}_\perp)}{E^+-E_n(\vec{q}+\vec{g},\vec{k}_\perp)}\ . \tag{A1}$$

The sum over $\vec{g}$ runs only over a restricted set of reciprocal-lattice vectors: For a given $\vec{q}$ in the surface Brillouin zone, only those values of $\vec{g}$ must be included for which $\vec{q}+\vec{g}=\vec{k}_{||}$ lies inside the projection of the first bulk Brillouin zone (BBZ) onto the (110) surface. The summation over $\vec{k}_\perp$ runs over those values for which

$$\vec{k}=(\vec{k}_{||},\vec{k}_\perp)=(\vec{q}+\vec{g},\vec{k}_\perp)$$

lies inside the BBZ.

In Fig. 12 we show the SBZ together with the projection of the BBZ onto a (110) plane. Considering a $\vec{q}$ point at the right of the $\Gamma X'$ line, two reciprocal-lattice vectors have to be retained: $\vec{g}=\vec{g}_0$ and $\vec{g}=\vec{g}_2$. Similarly, for a $\vec{q}$ point at the left of $\Gamma X'$, $\vec{g}=\vec{g}_0$ and $\vec{g}=\vec{g}_1$ have to be retained.

Figure 13 shows the SBZ and the BBZ viewed along the q_y direction. For a given $\vec{q}$, the summation range over $\vec{k}_\perp$ can be deduced for each $\vec{g}$ value retained. However, it is easily seen that the double summation over $\vec{k}_\perp$ and $\vec{g}$ may be replaced by a single summation over $\vec{k}_\perp$, whose summation range is independent of the particular $\vec{q}$ value and where only the term corresponding to $\vec{g}=\vec{g}_0$ has to be retained. Indeed, for any reciprocal bulk lattice vector $\vec{G}$, one has

$$C^n_{\alpha\nu}(\vec{k})=C^n_{\alpha\nu}(\vec{k}+\vec{G})e^{i\vec{G}\cdot\vec{\tau}_\nu} \tag{A2}$$

and

$$E_n(\vec{k})=E_n(\vec{k}+\vec{G})\ . \tag{A3}$$

Let us choose for the $\vec{q}$ considered

$$\vec{G}=(-\vec{g}_2,\pm\sqrt{2}\pi/a)\ . \tag{A4}$$

In the term of the sum (A1) corresponding to $\vec{g}=\vec{g}_2$, we may now, by adding $\vec{G}$, rewrite $\vec{k}=(\vec{q}+\vec{g}_2,k_\perp)$ as $\vec{k}+\vec{G}=(\vec{q},k_\perp)$, where now $k_\perp$ runs over the intervals

$$\left[-\frac{\sqrt{2}\pi}{a},-\frac{\sqrt{2}\pi}{a}+\delta\right]$$

and

$$\left[\frac{\sqrt{2}\pi}{a}-\delta,\frac{\sqrt{2}\pi}{a}\right]\ .$$

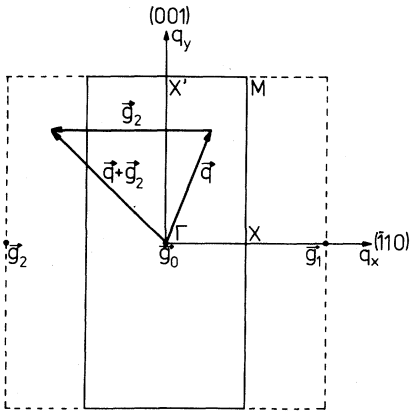

FIG. 12. Surface Brillouin zone of the (110) surface and projection of the bulk Brillouin zone on the (110) face (dotted lines).

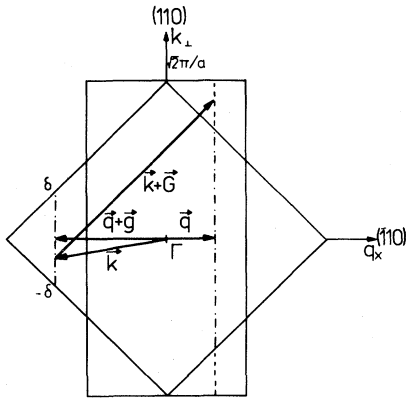

FIG. 13. Cut of the bulk Brillouin zone perpendicular to the (001) direction.

Thus combining the contributions from $\vec{g}=\vec{g}_0$ and $\vec{g}=\vec{g}_2$ is equivalent to retaining only the $\vec{g}=\vec{g}_0$ term, but extending the $k_\perp$ summation over the range

$$\left[-\frac{\sqrt{2\pi}}{a},+\frac{\sqrt{2\pi}}{a}\right].$$

The same argument holds for any $\vec{q}$ in the SBZ. Thus the sum (A1) may be rewritten

$$G^b_{ll'}(\vec{q},E)=\frac{N_2}{N_3}\sum_{k_\perp\in[-\sqrt{2\pi}/a,\sqrt{2\pi}/a]}\exp[i\vec{k}_\perp\cdot(\vec{\kappa}_m-\vec{\kappa}_{m'})]\sum_n\frac{C^n_l(\vec{q},k_\perp)C^{n*}_{l'}(\vec{q},k_\perp)}{E^+-E_n(\vec{q},k_\perp)}\ . \tag{A5}$$

We may replace the sum over $k_\perp$ by an integration according to

$$\sum_{k_\perp\in[-\beta,+\beta]}\rightarrow\frac{L_\perp}{2\pi}\int_{-\beta}^{\beta}dk_\perp\ ,$$

where we have defined $\beta=\sqrt{2}\pi/a$ and where $L_\perp$ is the length of the normalization volume along $k_\perp$. N_2 and N_3 are the number of points in the two- and three-dimensional Bravais lattices, respectively. Thus by examination of the surface unit cell (Fig. 3), one obtains for the ratio N_2/N_3

$$\frac{N_2}{N_3}=\frac{1}{L_\perp\sqrt{2}/a}\ . \tag{A6}$$

Inserting the preceding results into (A5) yields

$$G^b_{ll'}(\vec{q},E)=\frac{1}{2\beta}\int_{-\beta}^{\beta}\exp[ik_\perp(d_m-d_{m'})]\times\sum_n\frac{C^n_l(\vec{q},k_\perp)C^{n*}_{l'}(\vec{q},k_\perp)}{E^+-E_n(\vec{q},k_\perp)}dk_\perp\ , \tag{A7}$$

which is the result of Eqs. (8), $d_m-d_{m'}$ being the distance between layers m and m'.

[1]A. R. Peaker and B. Horsley, Rev. Sci. Instrum. 42, 1825 (1971).

[2]H. Pink, L. Treitinger, and L. Vité, Jpn. J. Appl. Phys. 19, 513 (1980); T. Oyabu, J. Appl. Phys. 53, 2785 (1982).

[3]M. von Ortenberg, J. Link, and R. Helbig, J. Opt. Soc. Am. 67, 968 (1977).

[4]E. Bucher, Appl. Phys. 17, 1 (1978); A. K. Ghosh, C. Fishman, and T. Feng, J. Appl. Phys. 49, 3490 (1978); J. Shewchun, R. Singh, and M. A. Green, *ibid.* 48, 765 (1977).

[5]Z. M. Jarzebski and J. P. Marton, J. Electrochem. Soc. 123, 199 (1976); 123, 299 (1976); 123, 333 (1976).

[6]F. J. Arlinghaus, J. Phys. Chem. Solids 35, 931 (1974).

[7]J. L. Jacquemin and G. Bordure, J. Phys. Chem. Solids 36, 1081 (1975).

[8]J. Robertson, J. Phys. C 12, 4767 (1979).

[9]E. de Frésart, J. Darville, and J. M. Gilles, Solid State Commun. 37, 13 (1981); Appl. Surf. Sci. 11-12, 259 (1982).

[10]I. Ivanov and J. Pollmann, Solid State Commun. 36, 361 (1980); Phys. Rev. B 24, 7275 (1981).

[11]J. Pollmann and S. T. Pantelides, Phys. Rev. B 18, 5524 (1978); J. Pollmann, in *Festkörperprobleme XX,* edited by J. Treusch (Vieweg, Braunschweig, 1980); I. Ivanov, A. Mazur, and J. Pollmann, Surf. Sci. 92, 365 (1980).

[12]M. Schmeits, A. Mazur, and J. Pollmann, Solid State Commun. 40, 1081 (1981); M. Schmeits, A. Mazur, and J. Pollmann, Phys. Rev. B 27, 5012 (1983).

[13]P. L. Gobby, Ph.D. thesis, Montana State University, 1977 (unpublished).

[14]D. Fröhlich, R. Kenklies, and R. Helbig, Phys. Rev. Lett. 41, 1750 (1978).

[15]V. T. Agekyan, Phys. Status Solidi 43, 11 (1977).

[16]W. A. Harrison, *Electronic Structure and the Properties of Solids* (Freeman, San Francisco, 1980).

[17]B. F. Levine, J. Chem. Phys. 59, 1463 (1973).

[18]D. H. Lee and J. D. Joannopoulos, Phys. Rev. B 24, 6899 (1981).